

The bright loop-top kernels in *Yohkoh* X-ray flares

J. Jakimiec¹, M. Tomczak¹, R. Falewicz¹, K.J.H. Phillips², and A. Fludra²

¹ Astronomical Institute of the Wrocław University, Kopernika 11, PL-51-622 Wrocław, Poland

² Rutherford Appleton Laboratory, Chilton, Didcot, Oxfordshire OX11 0QX, UK

Received 24 April 1997 / Accepted 19 February 1998

Abstract. We have investigated loop-top kernels of the soft X-ray emission seen in the *Yohkoh* Soft X-ray Telescope (SXT) images. Detailed comparison of the observations from various *Yohkoh* instruments shows that these kernels contain two kinds of flare plasma: a cooler (~ 10 MK) and a hotter (~ 20 MK) one. The cooler plasma plays a dominant role in the emission recorded by the SXT and the hotter plasma is responsible for the Fe XXV emission and the emission recorded by Hard X-ray Telescope 14–23 keV band during the post-impulsive phase of a flare. We argue that the best model, which is in agreement with the above observational results, is a turbulent model of a flare loop-top kernel. The magnetic field is tangled in the kernel and a number of transient current sheets occur there. The hotter (~ 20 MK) plasma is contained in the current sheets and they are surrounded by the cooler (~ 10 MK) plasma. The turbulent model of the flare loop-top kernel also allows us to explain why the kernels are brighter than the “legs” connecting them with the chromosphere.

Key words: Sun: corona – Sun: flares – Sun: X-rays, gamma rays

1. Introduction

A remarkable feature of soft X-ray flare images obtained with the Soft X-ray Telescope (SXT) on board the Japanese *Yohkoh* spacecraft is the presence of bright emission kernels or “knots” at or near the tops of loops (Acton et al. 1992; Feldman et al. 1994, 1995). For impulsive flares, the kernel diameters are 2 000 km or less (i.e. of the order of a single SXT pixel, or 1 800 km) and their heights $\lesssim 10\,000$ km, while for long-duration flares, their diameters are $\sim 10\,000$ km and heights $\gtrsim 50\,000$ km. X-ray images from instruments on the *Solar Maximum Mission* and *Hinotori* satellites also show such kernels, as do extreme ultraviolet spectroheliograms in Fe XXIII and Fe XXIV lines (estimated temperature ~ 11 MK, $1\text{ MK} = 1 \times 10^6$ K) that were taken with the US Naval Research Laboratory S082A instrument on the *Skylab* mission (Doschek & Feldman 1996). Because of the fact that the X-ray emission is

optically thin, it is possible to explain some of these bright emission kernels by purely geometrical effects (Alexander & Katsev 1996), but for some flares (e.g. Masuda 1994; Masuda et al. 1994, 1995) the geometry is apparently very simple and so the loop-top source seems to be real.

Flare temperatures can be obtained from the SXT observations using the ratio of emission through different X-ray filters, though more reliable values, as well as nonthermal velocities, are available from the Bragg Crystal Spectrometer (BCS) on *Yohkoh*. BCS temperatures are derived from the intensity ratio of dielectronic satellite lines to the nearby resonance lines of He-like Fe, Ca, and S ions. The BCS, which is an uncollimated spectrometer, has no spatial resolution, so that it is unclear whether the BCS spectra are emitted by the loop-top kernels seen in SXT images or by the rest of the loop structure (Doschek et al. 1995). Khan et al. (1995) have overcome this problem in their discussion of four flares observed by *Yohkoh* on the same date in an active region that was progressively more occulted by the Sun’s west limb. The SXT images reveal that the BCS emission was certainly from the loop-top kernel in each flare. A range of temperatures (from ~ 10 MK to ~ 20 MK) was derived from the BCS spectra, so supporting the conclusion of Doschek & Feldman (1996) from their *Skylab* study, and in addition significant nonthermal velocities (up to ~ 200 km s⁻¹) were found, not only at the start of each event but also well into the decay stages.

Jakimiec (1990) has investigated the heating of a flare plasma and how it is maintained at high temperature ($T_e \gtrsim 10$ MK) when calculations would suggest that the heat loss by thermal conduction is very high. He concluded that there must be a high degree of MHD turbulence in the region of energy release in the flare, indications for which are provided by the non-thermal line broadening in flare X-ray spectra. This idea was developed further (Jakimiec 1991; Jakimiec & Fludra 1991) and then the existence of loop-top kernels was becoming evident from the SXT observations. The suggestion was that the magnetic lines are tangled inside the flare kernels, but the lines which emerge from the kernels to form the legs of soft X-ray loops are noncomplex or “regular”.

We note that also in other astrophysical problems such tangled magnetic fields may be of importance, e.g. in clusters of galaxies (Sarazin 1986; Fabian et al. 1991).

Send offprint requests to: M. Tomczak

Table 1. List of investigated flare loop-top kernels (event numbers according Pike et al. 1996)

Event no.	Date	Integration Time	BCS Fe XXV diagnostics		SXT flare kernel		Flare coordinates
			T_e [MK]	EM [10^{48} cm^{-3}]	T_e [MK]	EM [10^{48} cm^{-3}]	
8	Dec 15, 1991	14:21:54-14:24:09	19	1.5	10.8	4.9	N06W40
11	Dec 18, 1991	10:25:06-10:31:33	20.5	4.0	8.1	7.4	S17Elimb ^a
12	Dec 26, 1991	07:34:03-07:36:33	20	2.7	12.7	7.8	S16W11
14	Dec 26, 1991	21:35:50-21:46:32	19.5	4.0	12.1	15.8	S15E25
15	Dec 27, 1991	06:10:11-06:15:47	18	4.3	13.5	7.0	S18E35
16	Dec 28, 1991	12:26:18-12:29:24	20	5.9	12.7	14.5	S18W37
20	Jan 13, 1992	17:25:34-17:34:28	19	2.3	11.1	7.6	S16Wlimb
21	Jan 30, 1992	02:27:50-02:32:29	19	1.6	11.8	4.5	S02W02
22	Feb 4, 1992	03:55:20-04:04:20	17	2.3	11.0	7.5	S06W60
26	Feb 6, 1992	20:50:37-20:59:06	20.5	4.1	12.4	10.0	N05Wlimb ^a
27	Feb 7, 1992	11:49:57-11:59:09	17.5	4.4	10.2	11.5	S17W50
30	Feb 17, 1992	15:40:25-15:46:01	18.5	2.5	10.6	8.2	N16W81
31	Feb 19, 1992	03:48:23-03:56:29	18	5.5	9.9	17.7	N04E82
32	Feb 19, 1992	14:44:35-14:53:50	18.5	0.7	14.4	1.1	N06Elimb ^a
35	Mar 15, 1992	01:52:22-02:10:55	17.5	7.7	9.8	43.1	S15E27
39	Jun 25, 1992	17:53:47-17:58:47	17.5	4.2	9.3	8.5	N09W69
41	Jul 3, 1992	09:45:57-09:53:45	18.5	2.0	12.5	5.0	N14E25
44	Jul 18, 1992	13:42:38-13:45:08	18.5	3.9	9.8	11.5	S08W90 ^a
45	Aug 11, 1992	22:25:17-22:29:11	19	2.5	10.2	4.0	N15E82
48	Aug 21, 1992	11:01:24-11:12:24	19	1.5	9.0	3.0	N14W44
50	Sep 5, 1992	11:24:20-11:26:08	19.5	1.7	14.2	3.1	S08W22
51	Sep 6, 1992	05:14:35-05:18:59	19	2.9	12.7	6.4	S10W40
52	Sep 6, 1992	09:02:48-09:07:21	20	4.8	11.1	12.4	S10W36
55	Sep 7, 1992	08:51:44-08:59:14	18	1.8	13.7	2.4	S10W54
56	Sep 9, 1992	02:06:57-02:14:06	19	3.0	10.4	11.8	S10W72
57	Sep 10, 1992	22:52:07-22:56:58	21	4.0	12.6	10.8	N12E41
58	Sep 11, 1992	02:54:56-03:01:05	18	1.5	10.9	8.7	N17E40
59	Oct 5, 1992	09:24:56-09:29:59	19	2.4	10.9	8.7	S07Wlimb ^a
61	Oct 19, 1992	17:55:10-17:58:19	17.5	2.2	10.6	4.4	N06E24
62	Oct 27, 1992	01:44:57-01:48:06	19	1.2	12.4	3.2	S25W18
64	Nov 5, 1992	06:19:20-06:21:53	18	4.0	10.4	10.0	S16W90 ^a
66	Feb 11, 1993	18:31:35-18:32:53	21	3.3	12.3	13.5	S04W16
68	Jun 7, 1993	14:12:30-14:20:27	22	2.0	14.0	4.9	S10W30
71	Sep 27, 1993	12:08:06-12:13:45	21	2.1	10.3	10.0	N08E90
72	Oct 9, 1993	08:08:23- 08:11:11	20	1.8	11.9	3.7	N12W74
75	Dec 25, 1993	17:54:29-17:56:20	23	1.4	14.0	6.8	N07E06

^a Limb flares with footpoints occulted by the Sun

In this paper we analyze a large number of flares for which high-quality *Yohkoh* observations exist, and present further evidence that the flare emission observed by the BCS arises primarily from the loop-top kernel as seen with the SXT. The differences in temperature derived simultaneously from the BCS and SXT therefore show that the loop-top kernels are multithermal, confirming Khan et al. (1995) and Doschek & Feldman (1996). In addition, we show that the kernel emission seen at higher energies (14–23 keV) with the *Yohkoh* Hard X-ray Telescope (HXT) is also related to the BCS and SXT emission. Implications for an MHD-turbulent picture of the flare are then discussed.

2. The *Yohkoh* instruments

The SXT on *Yohkoh* (Tsuneta et al. 1991) is a grazing-incidence telescope sensitive to 3–50 Å X-rays, having a CCD detector and filters to provide wavelength discrimination. Those sensitive to the highest energies are a 119 μm beryllium filter (Be119) and a 11.6 μm Al filter (Al12). The ratio of emission observed with these two filters gives temperature and emission measure. The BCS (Culhane et al. 1991) is an uncollimated spectrometer consisting of four curved Bragg-diffracting germanium crystals, each viewing X-ray lines of diagnostic importance. These include He-like Fe (Fe xxv) lines at ~ 1.85 Å, H-like Fe (Fe xxvi) lines at ~ 1.79 Å, He-like Ca (Ca xix) lines at ~ 3.18 Å, and He-like S (S xv) lines at ~ 5.04 Å. Electron temperatures T_e and emission measures can be deduced

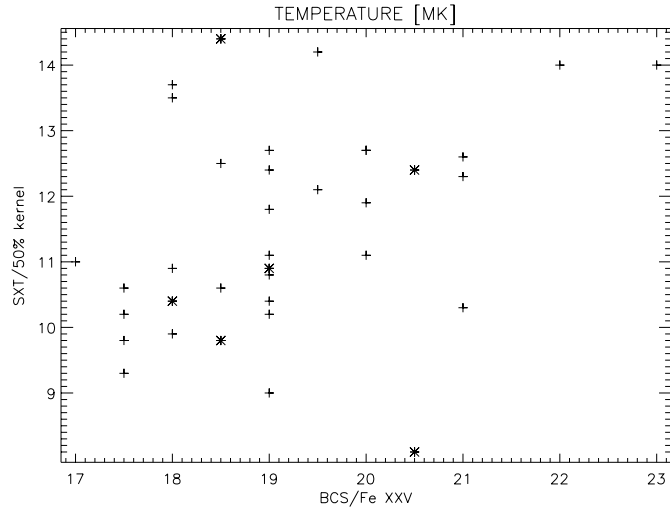


Fig. 1. Comparison of the temperatures obtained for the SXT flare loop-top kernels and derived from BCS Fe XXV spectra for events from Table 1. Typical uncertainties in the BCS temperatures are estimated to be 1.0 MK and in SXT temperatures 0.5 MK.

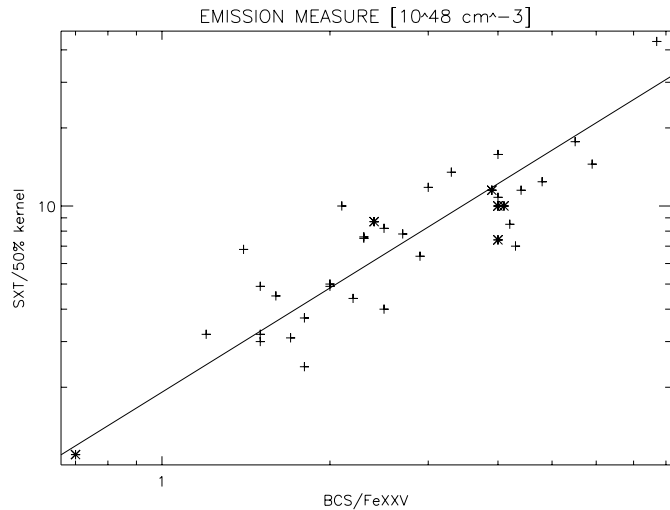


Fig. 2. Correlation between the emission measures obtained for the SXT flare loop-top kernels and derived from BCS Fe XXV spectra for events from Table 1. A typical relative error is about 30% for BCS, and about 15% for SXT. Linear least-squares fit to the data is shown as a continuous line.

from the intensity ratios of dielectronic satellite lines in each spectral region to the resonance line of each ion. The HXT (Kosugi et al. 1991) is a Fourier-synthesis hard X-ray imager which measures spatially modulated intensities from 64 independent subcollimators. Images are constructed from the data by the maximum entropy method or other procedures. There are four energy bands (L: 14–23 keV, M1: 23–33 keV, M2: 33–53 keV, and H: 53–93 keV). The angular resolution is up to ~ 5 arc sec and time resolution 0.5 s. Our analysis of the data from these instruments was done with standard software described by Morrison (1994).

Table 2. Effective SXT temperatures estimated for two-component model of the loop-top kernel

q	0.0	0.1	0.2	0.3	0.4	0.5	0.6	0.7	1.0
T	10.0	10.7	11.3	11.8	12.2	12.6	13.0	13.4	14.2

3. Analysis of the *Yohkoh* observations

3.1. Flare selection and initial analysis

Pike et al. (1996) studied 75 flares observed with the BCS between 1991 and 1993 which have detectable Fe XXVI line emission. Fe XXV and Fe XXVI spectra were analyzed to derive temperatures T_e (BCS) and emission measures ε (BCS) for small time intervals (ranging from less than 1 minute to about 20 minutes) near flare maximum, but avoiding periods near the flare onset when X-ray line profiles are generally highly broadened. Temperatures of about 20 MK were obtained from the Fe XXV spectra, and about 20–35 MK from the Fe XXVI spectra. As the Fe XXVI spectra were generally weak, the uncertainties in the Fe XXVI temperatures are much larger than those in the Fe XXV spectra.

In order to investigate any relation of the BCS Fe XXV temperatures and emission measures to the SXT emission, we first defined the soft X-ray kernels in the SXT Be119 filter images at flare maximum as the emission within areas outlined by the isophote that is 50% of the brightest pixel, generally located near the loop top. Example of the SXT flare kernel is shown in Fig. 4. Temperatures T_e (SXT) and emission measures ε (SXT) of the total radiation within the kernel area were then found from the ratio of intensities in the Be119 and Al12 filters. This was done for the same time interval over which the BCS observations were made, given by Pike et al. (1996). We found that SXT data were not available for some flares in the Pike et al. (1996) list for exactly these time intervals, this being the main reason why only 36 of the 75 flares were selected. The values of T_e (SXT) and ε (SXT) for the 36 flares are given in Table 1. In this table are also flare coordinates which are the H α flare coordinates from Pike et al. (1996) except for those marked “limb” which are from SXT images (these include cases where the loop-top kernel was off the limb). It can be seen from Table 1 that the temperatures of the flare kernels are systematically lower, and the emission measures higher, than those obtained from the BCS Fe XXV spectra.

The temperatures derived from the SXT data can underestimate the true temperatures owing to differences in the widths of the Point Spread Function (PSF) between the Be119 and Al12 filter energy bands. This effect is estimated in the Appendix. It is shown that the effect is significant only for very small loop-top kernels but not for those investigated in the present paper since the kernel sizes (FWHM) were generally ≥ 3 pixels.

3.2. Comparison of BCS data and the SXT data

We first plotted the SXT flare loop-top kernel temperatures against those derived from the BCS Fe XXV spectra for the 36

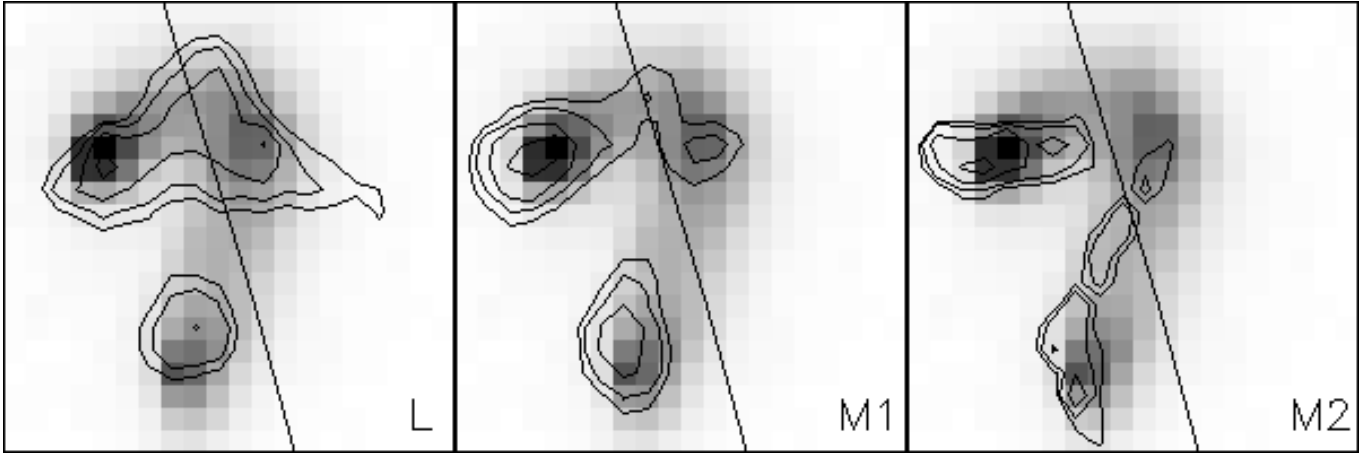


Fig. 3. The SXT(Be119) image (grey scale) of 17 February 1992 flare made at 15:41:01 UT. The field of view is 49 arc sec \times 49 arc sec. Solar north is up, east to the left. Contours of the HXT emission (78.4, 39.2, 19.6 and 11.8 % of the maximum intensity) for the channels L, M1 and M2 are overlotted. The continuous curve represents the solar west limb.

flares given in Table 1 (Fig. 1). The size of estimated uncertainties, mainly due to statistical variations in the count rates in each case, amount to less than about 1.0 MK for BCS temperatures and between 0.5 MK for SXT temperatures. No correlation was evident although the total range of temperatures is only about 5 MK in each case.

We then plotted the emission measures derived from the SXT and BCS temperatures (Fig. 2). The estimated uncertainties based on the stated temperature uncertainties are about 30% for BCS emission measures and about 15% for SXT emission measures. For this plot, there is a very good correlation, with almost all points falling within a factor 2 of the least-squares line which is also shown. The scatter of the points is most probably due to physical differences between the flare loop-top kernels (the scatter is larger than estimated statistical uncertainties). The least-squares line has the functional relation

$$\log \varepsilon(\text{SXT}) = (0.28 \pm 0.04) + (1.34 \pm 0.13) \times \log \varepsilon(\text{BCS})$$

Note that these flares include those which are at or outside the solar limb and have their loop footpoints occulted by the Sun (points marked by asterisks). These points show no systematic deviation from the other ones and this shows that the footpoint contribution to the Fe XXV emission observed by the BCS is of small importance. This near-proportional relation between the emission measures indicates the hotter ($T_e \sim 20$ MK) and cooler ($T_e \simeq 10 - 15$ MK) plasmas co-exist within the flare loop-top kernels and that there is a close physical relation between them.

3.3. The hot plasma contribution to the SXT observations

For temperatures $T_e \sim 10$ MK, the SXT Be119 and A112 filter responses are weakly dependent on temperature (see Fig. 9 in Tsuneta et al. 1991). It is not therefore clear whether plasma at higher temperatures, e.g. $T_e \sim 20$ MK, has a significant effect in the SXT emission.

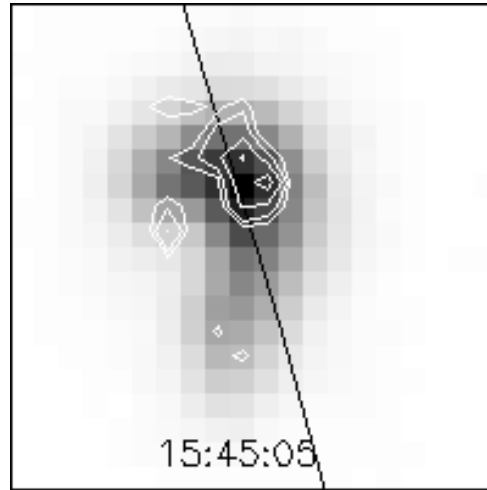


Fig. 4. The SXT(Be119) image (grey scale) of 17 February 1992 flare made at 15:45:05 UT. Contours of the HXT(L) emission are overlotted. For other details, see the caption of Fig. 3.

In this section we show that the SXT is not very sensitive to the hot ($T_e \sim 20$ MK) plasma observed by the BCS Fe XXV channel. In order to investigate this effect quantitatively, we carried out the following simple calculations. We assumed that the characteristic temperature of the cooler component is $T_1 = 10$ MK and of the hotter component is $T_2 = 20$ MK and the emission measures are ε_1 and ε_2 respectively. We have calculated the “effective temperature” \tilde{T} of the loop-top kernel from the formula:

$$\frac{f_B(\tilde{T})}{f_A(\tilde{T})} = \frac{f_B(T_1)\varepsilon_1 + f_B(T_2)\varepsilon_2}{f_A(T_1)\varepsilon_1 + f_A(T_2)\varepsilon_2} \quad (1)$$

where $f_B(T)$ and $f_A(T)$ are the response functions for the Be119 and A112 filters.

In Table 2 the values of \tilde{T} are given as a function of the ratio $q = \varepsilon_2/\varepsilon_1$ of the emission measures. We see that the effective temperature of an SXT loop-top kernel remains small

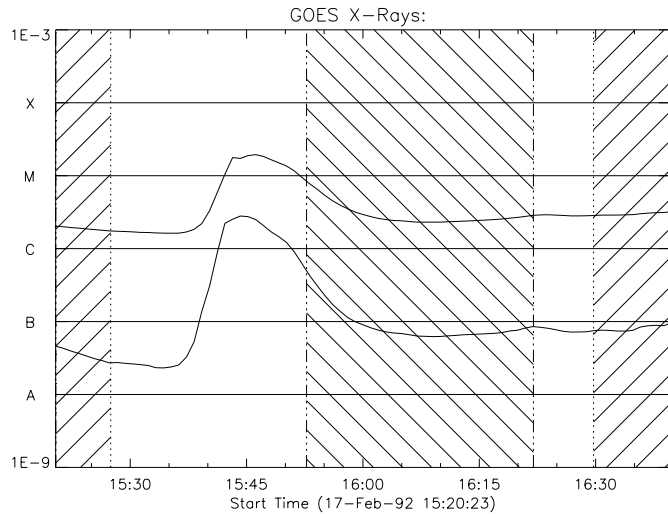


Fig. 5. The GOES light curves for the 17 February 1992 flare. Emission in the 1–8 Å band is shown by the upper curve, that in the 0.5–4 Å band by the lower curve. Time intervals shown by the hatched areas indicate times when BCS data were unavailable because of either satellite nighttime or South Atlantic Anomaly passages.

($T_e \leq 13$ MK) even for a very significant hot plasma component having $q = 0.5$. The values of $q = \varepsilon_2/\varepsilon_1$ suggested by the data in Table 1 fall within the range 0.2–0.6, with mean value of 0.40, and so we can be reasonably sure that the contribution of the relatively hot plasma that the BCS instrument is sensitive to is minor.

On the other hand, the Fe XXV line emission comes entirely from the hot component owing to the very steeply increasing temperature dependence of the emissivity in the $T_e \leq 20$ MK range.

3.4. Investigation of the X-ray images

Hereafter we concentrate our attention on flares having simple structure in soft X-rays (SXR). An example of such a flare is shown in Figs. 3 and 4. A flaring loop is seen in the SXR (grey scale) with the loop-top kernel seen above the solar limb and the loop footpoints on the solar disk. This structure is also clearly seen in hard X-ray (HXR) images which are shown as contours. At the flare beginning the footpoints were brighter than the loop-top kernel both in SXR and HXR (Fig. 3), but the loop-top kernel continued to brighten in the SXR during flare growth so that it was the brightest part of the flare near the SXR flare maximum (Fig. 4).

Soft X-ray (GOES) and hard X-ray (*Yohkoh* HXT) light curves of this flare are shown in Figs. 5 and 6 respectively. $H\alpha$ flare lasted from 15:42 to 15:53 UT, so its duration was about 11 minutes (Solar-Geophysical Data). The $H\alpha$ flare was seen as a small and weak subflare (SF) having an apparent area of 47×10^{-6} solar disk and its centre was located at N16 W81, at the northern (brighter) X-ray flare footpoint.

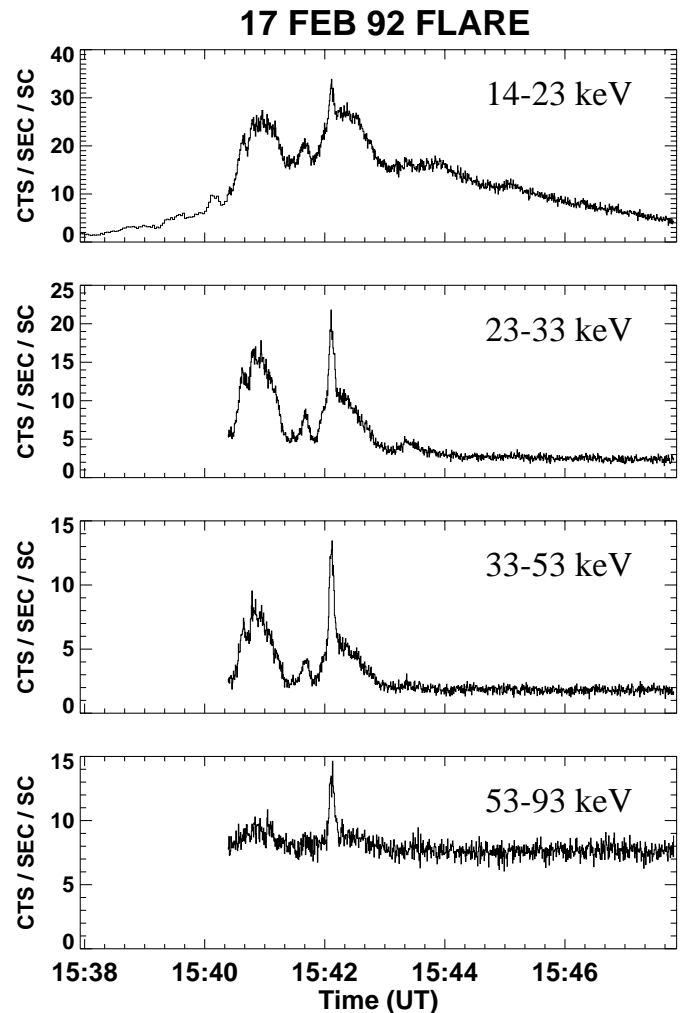


Fig. 6. The HXT light curves for the 17 February 1992 flare.

Another good example of such a flare having simple geometry is the flare of 13 January 1992 comprehensively investigated by Masuda (1994).

A general survey of *Yohkoh* observations shows that many small flares (GOES class C or low class M) also have a simple structure in soft X-rays, i.e. we see a loop with bright loop-top kernel and footpoints during the impulsive phase and the loop-top kernel is the dominant source later on (Acton et al. 1992). Their characteristic feature is also short duration in $H\alpha$ ($\Delta t \lesssim 10$ min) and in soft X-rays ($\Delta t \lesssim 20$ min). They have a steep decay phase. They are characterized by a single bright emission source at the top of the loop, which we refer to here as the loop-top kernel. We believe this to be the site of energy release (see Sect. 3.6). When the loop-top kernel ceases to be visible, the total flux of the flare quickly decays. In large, long-duration flares usually we have two or more soft X-ray sources (emission kernels). During the decay of the first source at least one other flare kernel develops, which is usually larger and higher than the first one, and this second kernel (or kernels) causes the flare's slow decay (Jakimiec & Fludra 1991).

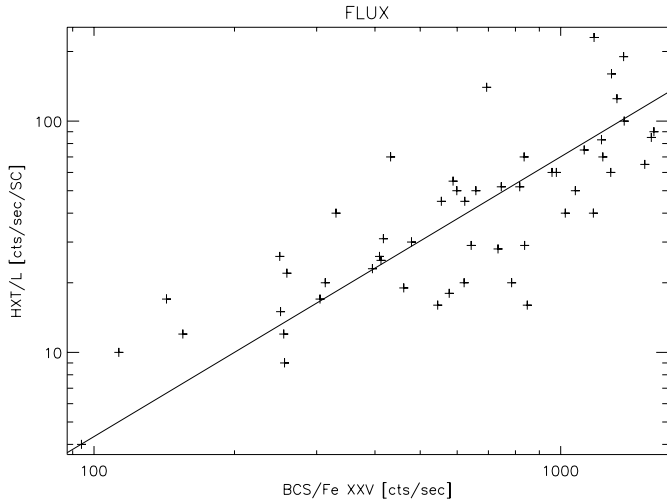


Fig. 7. Correlation between the BCS Fe XXV line photon count rates and the HXT (L channel) photon count rates for the investigated flares. The least-squares linear fit to the data is shown as a continuous line. The statistical errors for both HXT and BCS are only a few per cent. The large dispersion of the points is due to the difference between the BCS Fe XXV and HXT(L) response functions $f_i(T)$.

In Fig. 4 we see that after the impulsive phase the HXR emission in the HXT low energy band (14–23 keV) comes from the loop-top kernel. This result was first obtained by Masuda (1994), who found that this is true for all ten flares investigated by him. During the post-impulsive phase the 14–23 keV emission is quasi-thermal in origin coming from hot plasma with $T \gtrsim 20$ MK (Masuda 1994). So this result is an important confirmation that the hotter flare plasma component is located in the loop-top kernels.

In addition, in Fig. 7 the total HXT(L) photon count rates for the post-impulsive phases are compared with the BCS Fe XXV photon count rates for all investigated flares. There is generally a good correlation, confirming that both kinds of emission come from the same hot plasma component contained in the flare loop-top kernels.

3.5. Investigation of the SXT temperature maps

We have selected a number of SXT flares having single loop-top kernels. Using Be119 and Al12 images and standard SXT procedures we calculated the temperature and emission measure for each pixel, forming detailed SXT temperature and emission measure maps. In Figs. 8 and 9 we show examples of such maps for the 17 February 1992 flare and for another flare of 28 December 1991. The latter flare is a small subflare (SF) on the solar disc (S18 W37). The $H\alpha$ flare lasted from 12:29 UT to 12:37 UT, so its duration was about 8 minutes (Solar-Geophysical Data) and its SXR light curves (GOES) are shown in Fig. 10.

The most striking features of the temperature maps of all investigated loop-top kernels are that there is no temperature maximum at their centres and that within them the temperature $T(\text{SXT})$ is nearly uniform. This means that: (1) there is no concentration of the energy release, E_H , at the centres of the

kernels (see Sect. 3.7); (2) the transfer of the energy across the kernels is efficient.

A few pixels with higher temperatures do occur near the edges of and outside the loop-top kernels. These pixels, especially those with spuriously high values (> 20 MK), are at least partly due to instrumental effects: (1) the central core of the Point Spread Function (PSF) for the SXT Be119 filter is somewhat broader than for the Al12 filter (Martens et al. 1995), and this causes a systematic increase in the $I(\text{Be119})/I(\text{Al12})$ ratio at the outer edges (see Appendix); (2) small errors in the coalignment of the Be119 and Al12 images can produce significant deviations in temperature estimates near loop-top kernel edges (Siarkowski et al. 1996). A part of the effect of the temperature increase at the kernel edges should, however, be a real physical effect due to the fact that the energy release is enhanced there (see Sect. 3.7).

In order to compare these temperature maps with the results of the BCS diagnostics we have summed up the emission measures of the pixels having high temperature in the SXT temperature maps. The results for the flare of 28 December 1991 are shown in Fig. 11 where it can be seen that the emission measure at $T \geq 16$ MK never exceeds $3 \times 10^{48} \text{ cm}^{-3}$. The average BCS values for the time interval 12:26:18–12:29:24 UT are: $T \simeq 20$ MK, $\varepsilon \simeq 6 \times 10^{48} \text{ cm}^{-3}$, see Table 1. We see that the obtained SXT emission measures are significantly lower than those from the BCS Fe XXV spectra. This means that the hotter pixels seen in the SXT maps cannot be responsible for the whole Fe XXV emission. Large part of the hotter plasma (~ 20 MK) should be contained inside the flare loop-top kernel where it should be mixed with the cooler (~ 10 MK) plasma.

More examples of SXT flare loop-top kernels will be discussed in another paper.

3.6. A turbulent magnetic field model for the flare loop-top kernel

If the magnetic field inside a flare loop-top kernel had a regular topology, the energy transport across the magnetic lines of force would be practically inhibited, so that the temperatures could not be equalized across the lines of force in the relatively short lifetimes of solar flares. Therefore the fact that $T(\text{SXT}) \simeq \text{const}$ inside the flare kernels strongly suggests that the magnetic field is not regular there but rather is turbulent with many reconnection regions occurring in which energy release takes place to heat the plasma.

Jakimiec (1990) has also shown that plasma cannot be efficiently heated up to temperatures ~ 10 MK in laminar current sheets because of very high efficiency of the thermal conductivity along the regular magnetic lines of force. He came to the conclusion that the region of energy release should be turbulent. Thus the high temperature of the flare plasma is also a strong indication that the region of the flare energy release is turbulent.

In high-resolution SXR spectra of all flares a significant non-thermal line broadening (NTLB) occurs, i.e. the line widths are larger than the widths due to thermal motions scheme (Antonucci et al. 1982; Fludra et al. 1989). It is important that the

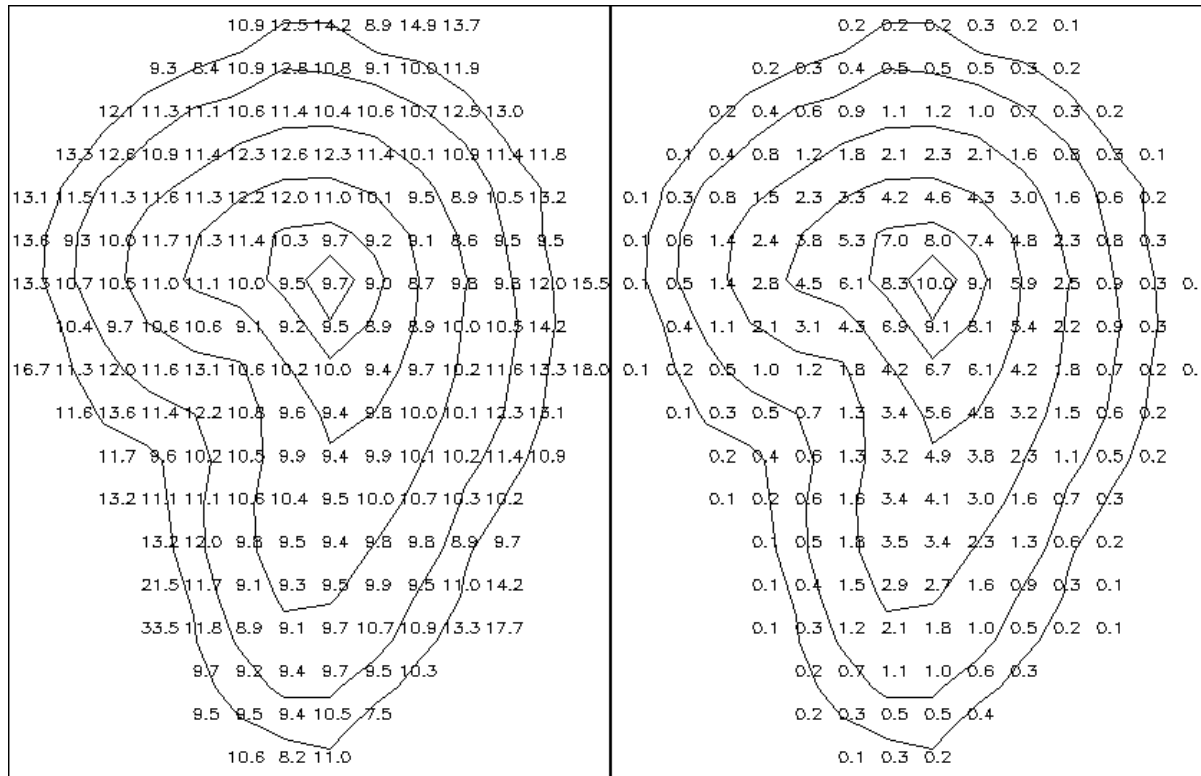


Fig. 8. An example of the temperature (left) and emission measure (right) map for the flare of 17 February 1992, for 15:45:05 UT. In both maps each pixel is $2.45 \text{ arc sec} \times 2.45 \text{ arc sec}$. North is at the top, east – to the left. Temperature units are MK, emission measure units are 10^{47} cm^{-3} . Contours represent the Be119 intensities at 90, 75, 50, 25, 10 and 5 % of the brightest pixel.

NTLB occurs in all flares and has similar amplitudes independent on their position on the solar disc and on their orientation relative to the observer’s line of sight. We think that this is a strong indication that at least a part of the observed NTLB is due to random (turbulent) plasma motions. The turbulent velocities, v_t , as derived from the non-thermal line broadening in the BCS Fe XXV spectra for the two above investigated flares, are shown in Figs. 12 and 13 (bottom panels).

Taking the above arguments together, we conclude that the flare loop-top kernels are turbulent, i.e. the magnetic field lines are tangled and with many transient, turbulent current sheets being formed. A possible model for the flare magnetic field geometry, based on Jakimiec (1991), is illustrated in Fig. 14. In this, the flare kernel is connected to the chromosphere by loop legs having a regular topology.

This model allows us to explain why the loop-top kernels are usually brighter than the legs. The point is that not all the magnetic lines in the legs are well connected with the interior of the turbulent kernel, so that heat flows in the legs only along certain lines of force. This is schematically explained in Figs. 15 and 16. In Fig. 15 the transition between the tangled magnetic field lines inside a loop-top kernel and the regular external (legs) field is shown schematically. In the figure only the lines of force have been drawn, along which the energy can easily flow out from the kernel due to their good connection with the interior of the kernel. In Fig. 16 is shown an external line of force which is

tangential to the kernel (Fig. 16a). And after a reconnection with an appropriate internal magnetic line the external line (or, more precisely, a bundle of lines of force) can get good connection with the kernel interior, allowing efficient energy outflow along this bundle (Fig. 16b).

As a result of such a magnetic modulation of the energy outflow from the loop-top kernel to the legs, the emission measure filling factor α_l for the legs will be usually smaller than the filling factor for the kernel α_k , so accounting for it being brighter. We estimate that typical values of the filling factor ratio near the flare maximum is $\alpha_l/\alpha_k \sim 0.1$.

In the case when the magnetic connection between the loop-top kernel and the legs is very good, $\alpha_l \simeq \alpha_k$ and we will see a more uniformly bright X-ray flare loop, i.e. with no bright kernel, this being the case for some small flares.

This model (loop-top kernel plus legs) easily explains also the cases when only one leg is seen or when plasma inflow to the flare kernel due to chromospheric evaporation is slow. These cases can be explained by low efficiency of the kernel/leg magnetic connection in one or both legs.

3.7. Distribution of the heating function in flare loop-top kernels

The SXT temperature maps allow us to investigate the distribution of the heating function, E_H , i.e. the rate of thermal energy

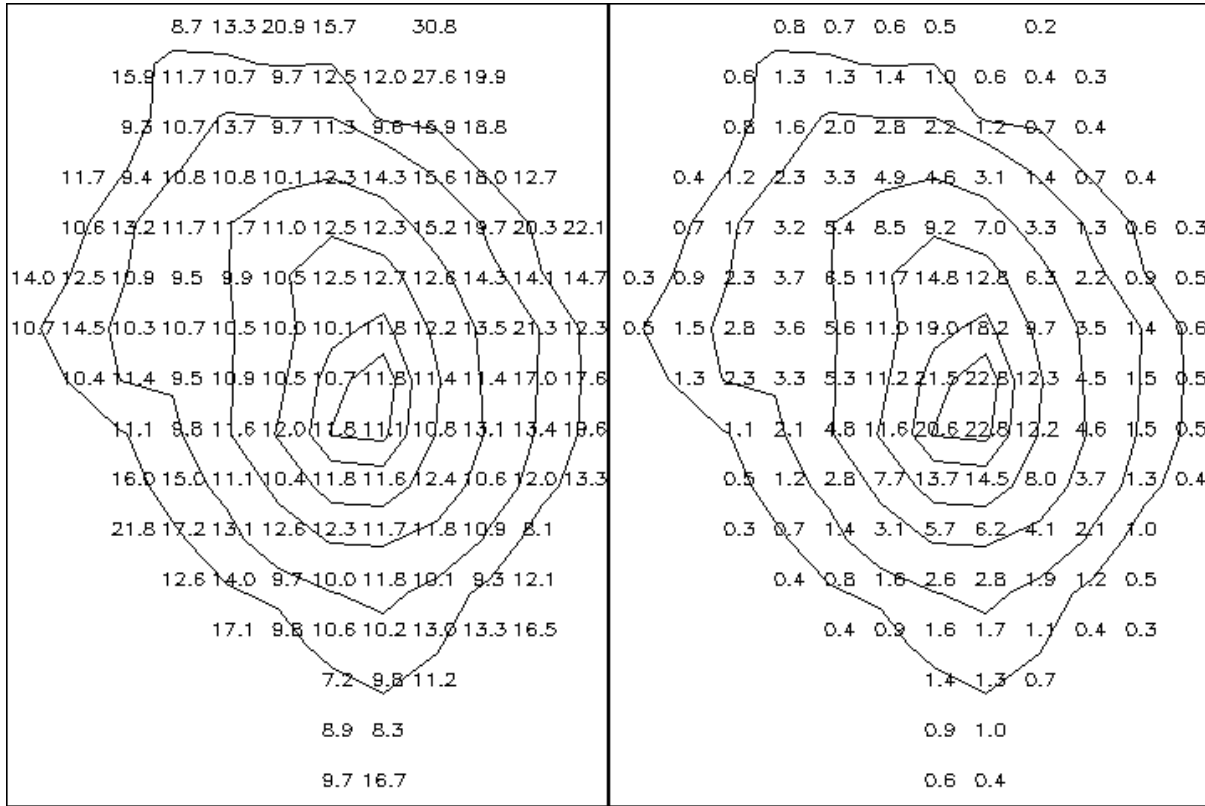


Fig. 9. An example of the temperature (left) and emission measure (right) map for the flare of 28 December 1991, for 12:28:56 UT. For other details, see the caption of Fig. 8.

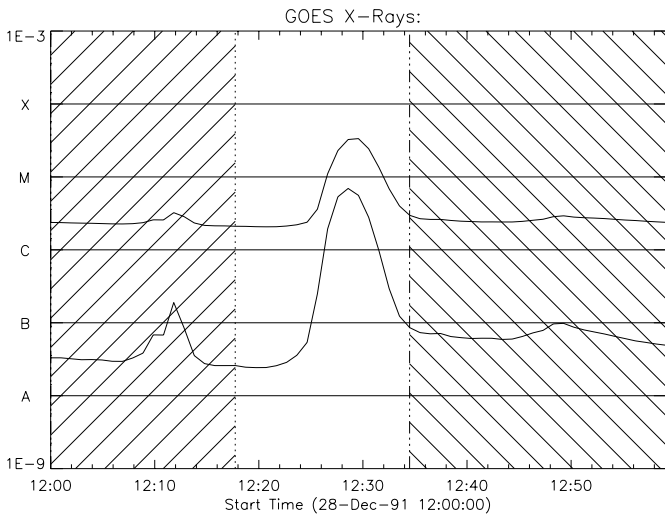


Fig. 10. The GOES light curves for the 28 December 1991 flare. For other details, see the caption of Fig. 5.

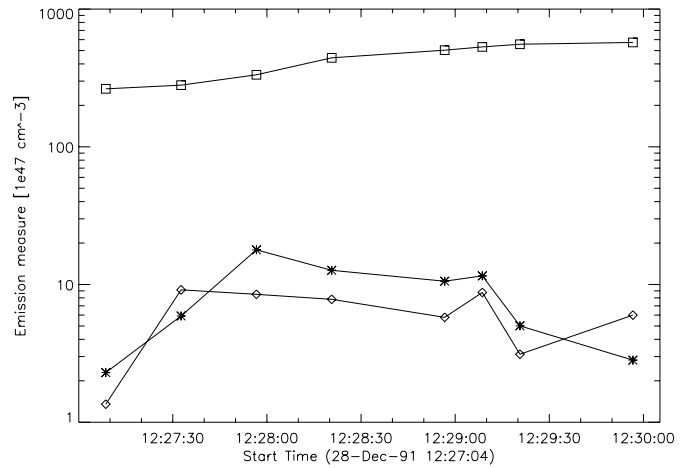


Fig. 11. Time variation of the emission measure of all pixels having temperature below 16 MK (boxes), between 16 and 20 MK (asterisks) and above 20 MK (diamonds) in the SXT temperature maps for the 28 December 1991 flare.

release per unit volume, in flare loop-top kernels. For this purpose we use the following simple model. The energy balance inside a flare kernel can be approximately described by the following formula:

$$\text{div}\mathbf{F} = E_H - E_R \tag{2}$$

where \mathbf{F} is the energy flux transferred by the turbulent motions and E_R is the total radiative energy loss ($\text{erg cm}^{-3} \text{ s}^{-1}$).

We assume a spherical symmetry of the kernel and in this section $E_H(r)$, $E_R(r)$ and $T(r)$ are considered to be averaged over the turbulence inhomogeneities.

$$\frac{1}{r^2} \frac{\partial(r^2 F)}{\partial r} = E'_H, \tag{3}$$

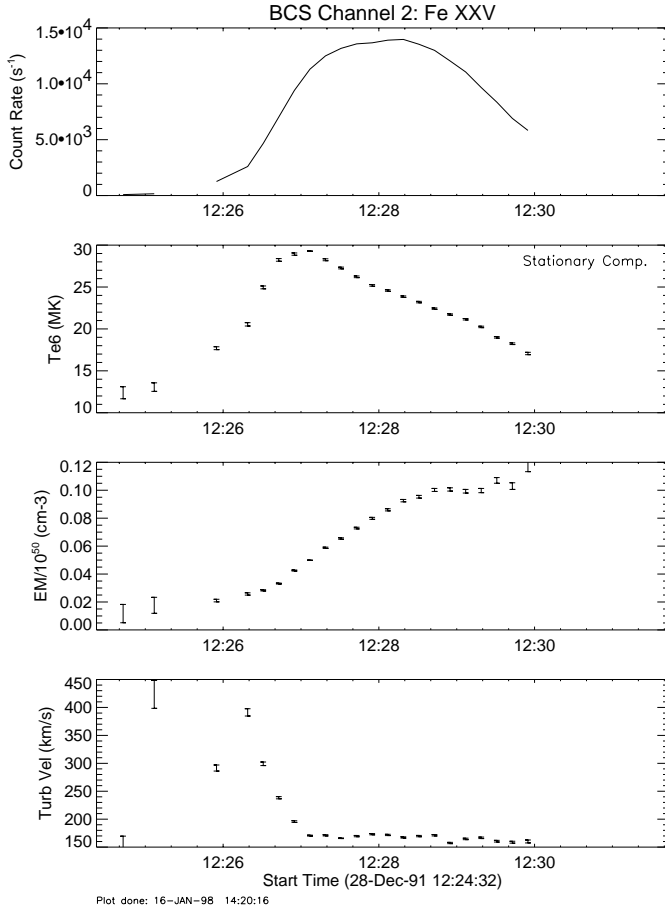


Fig. 12. Results of the BSC Fe XXV analysis for the 28 December 1991 flare.

where r is the radial variable and $E'_H = E_H - E_R$ is the “effective” heating rate. This gives:

$$F = \frac{1}{r^2} \int_0^r E'_H r'^2 dr \quad (4)$$

We will assume energy transport is by turbulence, with negligible amount by conduction. The energy flux is then given by

$$F = -\kappa_t dT/dr \quad (5)$$

where dT/dr is the temperature gradient and $\kappa_t = \rho c_p \bar{v} l / 2$ is the coefficient of energy transport by turbulence. Here ρ is the density, c_p is the specific heat at constant pressure, l is mixing length, i.e. the length over which energy is transported by turbulent elements most efficiently and \bar{v} is their mean velocity. By combining Eqs. (4) and (5), we obtain

$$\frac{dT}{dr} = -\frac{1}{\kappa_t r^2} \int_0^r E'_H r'^2 dr \quad (6)$$

For the specific case of homogeneous heating, $E'_H = const$, it will be:

$$\frac{dT}{dr} = -\frac{1}{3} \frac{E'_H}{\kappa_t} r \quad (7)$$

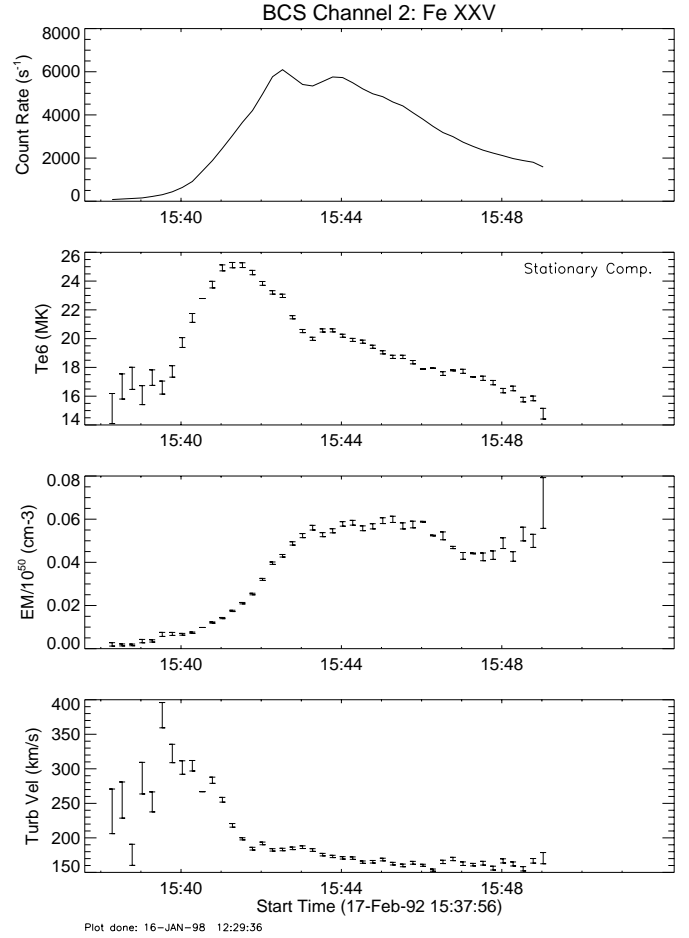


Fig. 13. Results of the BSC Fe XXV analysis for the 17 February 1992 flare.

and hence:

$$T(r) = T_0 - \Delta T (r/R)^2, \quad (8)$$

where $\Delta T = (1/6)(E'_H/\kappa_t)R^2$, T_0 is the temperature at the centre of the loop-top kernel and R is its radius. This means that in the case of uniform heating there should be a maximum of the temperature at the centre of a kernel and a continuous decrease of the temperature towards the edge.

In our SXT temperature maps we do not see any trace of such a temperature maximum at the centre. Hence we conclude that the heating function E_H is not uniformly distributed inside the loop-top kernels, but rather it should be enhanced near their edges. The simplest such heating function giving an isothermal distribution:

$$E'_H = \begin{cases} 0 & \text{for } 0 \leq r \leq r_1 \\ const & \text{for } r_1 \leq r \leq R \end{cases} \quad (9)$$

Note that $E'_H \approx 0$ does not mean zero heating in the central part of kernel, but rather that $E_H \approx E_R$ i.e. the heating is comparable to the radiative losses.

We note that this kind of heating distribution (i.e. E_H enhanced near the edges) is in a good agreement with what we can expect for a turbulent loop-top kernel. At the edges the tangled magnetic field of the kernel interacts (reconnects) with an

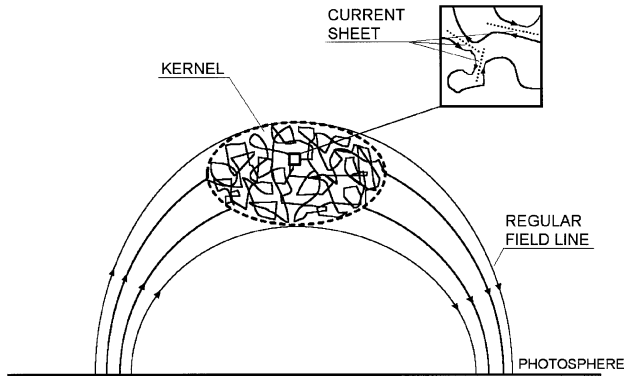


Fig. 14. Schematic diagram of the simple model of the turbulent flare loop-top kernel as discussed in Sect. 3.6. The magnetic field lines are regular along the loop legs but tangled in the kernel. Insert shows enlarged picture of reconnecting field lines (current sheets are shown as dotted lines).

external, regular magnetic field. The external magnetic field is somewhat stronger than the magnetic field inside the kernel, since the internal field has been decreased by multiple reconnections. Hence the heating near the edge can be expected to be stronger than the heating inside the kernel.

The increased temperatures at the kernel edges in the SXT temperature maps (see Figs. 8 and 9) can also be an evidence of the enhanced heating there.

4. Summary and conclusions

1. In the present paper we have collected arguments that flare loop-top kernels are turbulent regions (Sects. 3.2, 3.4, 3.6). In our model of a flare kernel the energy is released in many transient current sheets, in which plasma is hot ($T \gtrsim 20$ MK). After magnetic field reconnection the hot plasma mixes with the surrounding plasma maintaining its temperature at $T \sim 10$ MK. The Fe XXV and quasi-thermal HXT (L-channel) emission comes from the hot component and the main contribution to the SXT emission comes from the cooler component.
2. In the investigated flare loop-top kernels the temperature distribution is flat, $T(\text{SXT}) \simeq \text{const}$, at the central parts of the kernels. This indicates that the sources of the energy release (current sheets) are enhanced near the kernel edges where the turbulence interacts with the stronger, external magnetic field (see Sect. 3.7).
3. The turbulent model also allows us to explain why the kernels are brighter than the “legs” connecting them with the chromosphere. The legs have lower plasma filling factors than the kernel, since not all the magnetic lines of the legs have a good connection with the magnetic field of the kernel (see Sect. 3.6).
4. In the present paper we concentrated our attention on flare loop-top kernels which can be described by spherically symmetric models. But in many kernels the maximum of the quasi-thermal HXT(L) emission is shifted toward a kernel edge. This indicates deviation from the spherical symmetry:

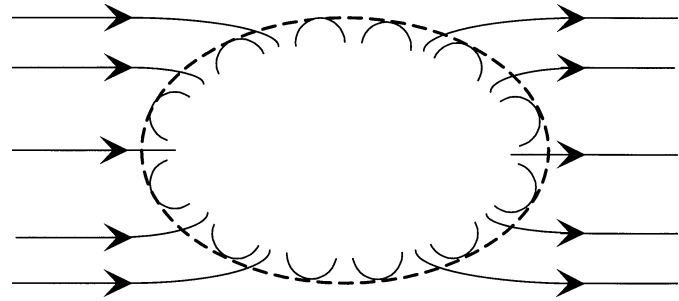
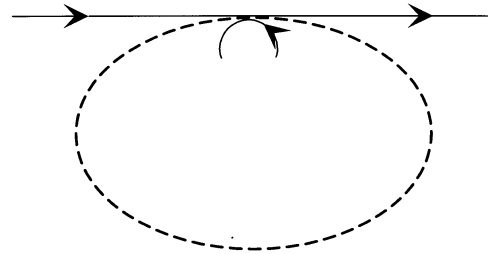


Fig. 15. A schematic diagram showing the transition between the turbulent region inside a flare loop-top kernel and the external laminar region. The dashed line shows the edge of the kernel. Thin lines inside the kernel are tangled magnetic lines of force. Outside the kernel only those lines of force have been drawn which have a good penetration into the kernel (thick lines with arrows). Along these lines will flow enhanced flux of energy.

(a)



(b)

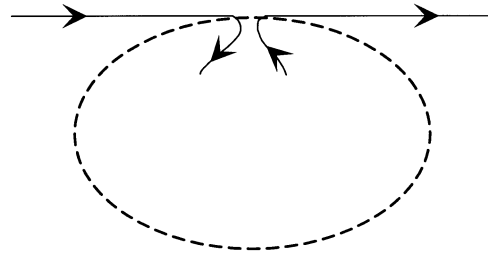


Fig. 16. a A schematic diagram showing the reconnection of an external line of force tangential to the loop-top kernel with an appropriate magnetic field inside the kernel. **b** As a result of the reconnection we will obtain lines of force well penetrating into the kernel.

the energy release is enhanced at the part of the edge, i.e. the current sheets are stronger (hotter) there. Examples of such kernels will be investigated in a next paper.

Acknowledgements. We acknowledge the hard work and dedication of the whole *Yohkoh* Team, which has made this research possible. The authors are very thankful to the referee, Dr. Brigitte Schmieder, for her valuable remarks which helped to improve the presentation of results. It is a pleasure to acknowledge financial contribution to this work by

Table A1. Values of the temperatures estimated from the SXT observations for the centre of flare loop-top kernel

FWHM of the kernel [SXT pixels]	1	2	3	4	5	6	7	8
T_{obs} [MK]	13.4	14.2	14.5	14.7	14.8	14.9	14.9	14.9

British Council/KBN collaborative grant (No. WAR/992/057) which has made the collaboration between Astronomical Institute of Wrocław University and Rutherford Appleton Laboratory possible. The Polish contribution has been supported by the Committee of Scientific Research (KBN) grant No. 2 P03D 016 14.

Appendix A: checking the flare loop-top kernel SXT temperatures

The width of the Point Spread Function (PSF) of the SXT changes somewhat with the radiation wavelength, being somewhat larger for the Be119 filter than for the Al12 filter (Martens et al. 1995). Because of this effect the temperatures determined for the central parts of loop-top kernels will be somewhat underestimated and they will be overestimated near their edges. In this section we show that this instrumental effect does not significantly influence the temperatures of the flare kernels determined from the SXT observations. In order to estimate this effect we assumed that the photometric profile of a kernel, as well as the PSF, can be approximated by the Gaussian functions, and applied a one-dimensional convolution of these functions.

Let the true distribution of X-ray intensities across a flare loop-top kernel (the photometric profile) be:

$$I_i^*(x) = \frac{a_i}{\sigma_i \sqrt{2\pi}} \exp\left(-\frac{x^2}{2\sigma_i^2}\right), \quad (\text{A1})$$

where $i = A, B$ for the observations with the Al12 or Be119 filters, respectively.

The central parts of the Point Spread Functions are approximated by the formulae:

$$f_i(x) = \frac{1}{\sigma_i \sqrt{2\pi}} \exp\left(-\frac{x^2}{2\sigma_i^2}\right), \quad (\text{A2})$$

where $i = A, B$. Then the observed photometric profiles should be:

$$I_i = \frac{a_i}{\sqrt{\sigma^2 + \sigma_i^2} \sqrt{2\pi}} \exp\left(-\frac{x^2}{2(\sigma^2 + \sigma_i^2)}\right) \quad (\text{A3})$$

and the ratio of the observed intensities at the centre of the kernel ($x = 0$):

$$\frac{I_B(0)}{I_A(0)} = \frac{a_B}{a_A} \sqrt{\frac{\sigma^2 + \sigma_A^2}{\sigma^2 + \sigma_B^2}} \quad (\text{A4})$$

We assumed that the temperature is 15 MK everywhere in the kernel, took the values σ_A and σ_B from Martens et al. (1995), calculated the observed ratio $I_B(0)/I_A(0)$ and converted it into the temperatures $T_{obs}(x = 0)$ which will be derived from the observed ratio:

$$\frac{f_B(T_{obs})}{f_A(T_{obs})} = \frac{I_B(0)}{I_A(0)} \quad (\text{A5})$$

where f_A, f_B are the SXT response functions for the Al12 and Be119 filters. The values of T_{obs} are given in Table A.1 as the function of the kernel size.

We see that the investigated instrumental effect is significant for small flare loop-top kernels (for FWHM = 1 pixel the estimated temperature will be 13.4 MK instead of 15 MK), but it is small for those with FWHM ≥ 3 pixels. It is clear that the investigated effect will decrease the estimated temperatures for the centre of a kernel, but it will increase them near its edge. We have estimated the latter effect for the isophote $0.1I_{max}$ in the kernel, using Eq. A.3. For the flare kernel of FWHM = 1 px we obtained $T_{obs} = 16.0$ MK and for FWHM = 3 px we obtained $T_{obs} = 16.2$ MK. The above estimates have been confirmed by two-dimensional numerical calculations (to be published in another paper).

References

- Acton L.W., Feldman U., Bruner M.E., et al. 1992, PASJ 44, L71
Alexander D., Katsev S. 1996, Sol. Phys. 167, 153
Antonucci E., Gabriel A.H., Acton L.W., et al. 1982, Sol. Phys. 78, 107
Culhane J.L., Hiei E., Doschek G.A., et al. 1991, Sol. Phys. 136, 89
Doschek G.A., Feldman U. 1996, ApJ 459, 773
Doschek G.A., Strong K.T., Tsuneta S. 1995, ApJ 440, 370
Fabian A.C., Nulsen P.E., Canizares C.R. 1991, A&AR 2, 191
Feldman U., Hiei E., Phillips K.J.H., Brown C.M., Lang J. 1994, ApJ 421, 843
Feldman U., Seely J.F., Doschek G.A., et al. 1995, ApJ 446, 860
Fludra A., Lemen J.R., Jakimiec J., Bentley R.D., Sylwester J. 1989, ApJ 344, 991
Jakimiec J. 1990, Adv. Space Res. 10(9), 109
Jakimiec J. 1991, paper presented to the XIV Consultation on Solar Physics, Karpacz, Poland, in press
Jakimiec J., Fludra A. 1991, Adv. Space Res. 11(5), 99
Kosugi T., Makishima K., Murakami T., et al. 1991, Sol. Phys. 136, 17
Khan J.I., Harra-Murnion L.K., Hudson H.S., Lemen J.R., Sterling A.C. 1995, ApJ 452, L153
Martens P.C., Acton L.W., Lemen J.R. 1995, Sol. Phys. 157, 141
Masuda S. 1994, Ph. D. thesis, University of Tokyo
Masuda S., Kosugi T., Hara H., Tsuneta S., Ogawara Y. 1994, Nat 371, 495
Masuda S., Kosugi T., Hara H., et al. 1995, PASJ 47, 677
Morrison M.D. 1994, *Yohkoh Analysis Guide*, Lockheed Palo Alto Research Laboratory
Pike C.D., Phillips K.J.H., Lang J., et al. 1996, ApJ 464, 487
Sarazin C.L. 1986, Rev. Mod. Phys. 58, 1
Siarkowski M., Sylwester J., Jakimiec J., Tomczak M. 1996, Acta Astron. 46, 15
Solar-Geophysical Data 574 II and 576 II, World Data Center A for Solar-Terrestrial Physics, Boulder, CO, USA
Tsuneta S., Acton L., Bruner M., et al. 1991, Sol. Phys. 136, 37